TOA Estimation Using UWB with Low Sampling Rate and Clock Drift Calibration

(Invited Paper)

Yiyin Wang * and Geert Leus *

Hakan Deliç *†

*Faculty of Electrical Engineering
Delft University of Technology
Mekelweg 4, 2628CD Delft, The Netherlands
Email: {yiyin.wang, g.j.t.leus}@tudelft.nl

†Wireless Communications Laboratory
Dept. of Electrical and Electronics Engineering
Bogaziçi University, Bebek 34342 Istanbul, Turkey
Email: delic@boun.edu.tr

***Abstract*—In this paper, a time-of-arrival (TOA) estimation scheme with clock drift calibration is proposed using an impulse-radio (IR) ultra-wideband (UWB) signal. We adopt low-rate stroboscopic sampling, which can achieve an equivalent sampling rate as high as the Nyquist sampling rate. The clock drift is one of the main error sources in TOA estimation for the stroboscopic sampling IR-UWB system, since a long preamble is required to collect sufficient data samples. Therefore, the drift is taken into account in our system model. First, the maximum-likelihood estimate of the drift is computed. Then, we employ the peak selection or the leading edge detection to estimate the TOA using the averaged data samples calibrated for the drift. Simulation results corroborate that the drift calibration significantly reduces the TOA estimation errors due to the drift, and that stroboscopic sampling can achieve the same estimation resolution as Nyquist sampling.**

I. Introduction

Ultra-wideband (UWB) radio is a promising technology for high resolution ranging [1]–[4]. To detect the first arriving component, we can estimate the time-of-arrival (TOA) with high resolution, which facilitates accurate ranging. In a line-of-sight (LOS) environment, the first path is usually the strongest one and we can perform peak selection [5], [6], whereas in a non-line-of-sight (NLOS) scenario, the first path normally is not the strongest one, in which case we have to set a threshold to detect the leading edge [5], [6].

Due to the large bandwidth of the impulse-radio (IR) UWB signal, its multipath channel components are resolvable. However, for the same reason the IR-UWB system requires a Nyquist sampling rate of several tens of GHz. This is prohibitively high for practical implementations. Most ranging systems [3], [7] are based on Nyquist sampling. Research has focused on sub-Nyquist sampling, using the stored reference (SR) correlator [5], the energy detector (ED) [5], or the transmitted-reference (TR) receiver [5], [8], where the noiseless template, the received signal itself, or its delayed version are used as templates for energy collection, respectively. In all these schemes, the accuracy of TOA estimation is sacrificed for sub-Nyquist sampling.

This research was supported in part by STW under the Green and Smart Process Technologies Program (Project 7976).

The purpose of this paper is to obtain a high resolution TOA estimate with low sampling rate. We make use of stroboscopic sampling, which is widely used in channel measurements [9]. It can obtain an effective sampling rate as high as several GHz using a low-rate sampler running at several tens or hundreds of MHz with the penalty of repetitively transmitting the same waveform. Since we have to transmit several identical pulses in order to collect the same samples as when transmitting one pulse sampled by an equivalent high sampling rate, the preamble for ranging is long. As a result, the clock drift, which refers to the phenomenon where the clock does not run at the nominal frequency, becomes one of the main error sources. Although a symmetric double-sided two-way ranging (SDS-TWR) protocol as in [1], [4] can reduce the ranging error due to clock drift significantly by relating the drift to the difference of the processing times at two devices instead of the processing time at one device, it can not calibrate for the TOA estimation error caused by the clock drift. A trellis-based maximum-likelihood crystal drift estimator is introduced in [10], [11] to solve this problem. However, the system sampling rate is still as high as several GHz. Furthermore, it does not consider the code mismatch due to the drift and the unknown TOA, which can cause serious problems. Therefore, we design a ranging preamble, solve the code mismatch problem and apply a maximum-likelihood estimator (MLE) to estimate the clock drift in our stroboscopic sampling IR-UWB system. After the drift calibration, the TOA estimation is carried out using peak selection or leading edge detection. Consequently, we calibrate for the timing error caused by the clock drift and achieve an accurate TOA estimate with low sampling rate.

The rest of this paper is organized as follows. In Section 2, we will first introduce the stroboscopic sampling principle. The clock drift is taken into account in the system model and the preamble is designed to facilitate the drift calibration. In Section 3, we propose a method to estimate the TOA with drift calibration. Simulation results are shown in Section 4. Conclusions are drawn at the end of the paper.

Notation: We use upper (lower) bold face letters to denote matrices (column vectors). $x(\cdot)$ $(x[\cdot])$ represents a continuous (discrete) time sequence. $\mathbf{X}(m,n)$, $\mathbf{X}(m,:)$ and $\mathbf{X}(:,n)$ de-

9781-4244-2931-8/09/$25.00 ©2009 IEEE

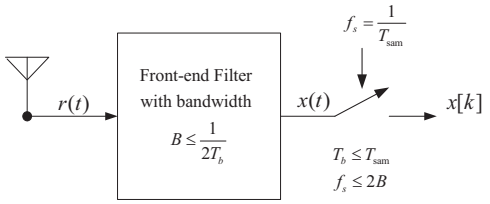

Fig. 1. The receiver's analog front-end. The output of the front-end filter is sampled at rate $1/T_{\text{sam}}$, which is smaller than its Nyquist sampling rate $2B$.

note the element on the mth row and nth column, the mth row, and the nth column of matrix $\mathbf{X}$, respectively. $\mathbf{0}_m$ ($\mathbf{1}_m$) is an all-zero (all-one) column vector of length m. Moreover, $(\cdot)^T$, $|\cdot|$, $\|\cdot\|_F$ and $\star$ designate transposition, absolute value, Frobenius norm and convolution, respectively. $\lfloor x \rfloor$ represents the largest integer smaller than or equal to x. All other notation should be self-explanatory.

II. System model

The preamble for ranging is composed of many frames. Each frame period T_f holds one pulse. We assume that T_f is larger than the delay spread of the channel in order to avoid inter-frame interference (IFI), e.g., $T_f = 100$ ns. The receiver employs a front-end filter to select the band of interest as shown in Fig. 1. The impulse response of the front-end filter does not have to be the received pulse shape, which is unknown due to the distortions caused by the channel and the antennas. For instance, it can be the transmitted pulse. In general, we specify the filter in the frequency domain in order to capture most of the signal energy in the band of interest. The bandwidth B of the front-end filter is quite large because of the bandwidth of the UWB signal. Hence, the Nyquist sampling rate becomes prohibitively high. For example, if we transmit pulses with a bandwidth of 500 MHz, a sampling rate of at least 1 GHz is required at the receiver. Therefore, we resort to stroboscopic sampling [9] to sample the output of the front-end filter at rate $1/T_{\text{sam}}$, which is much smaller than its Nyquist sampling rate $2B$, i.e., $T_{\text{sam}} \geq 1/2B$. Consequently, each frame produces in $\lfloor T_f/T_{\text{sam}} \rfloor$ or $\lceil T_f/T_{\text{sam}} \rceil$ samples.

Since we apply stroboscopic sampling, several identical frames have to be transmitted in order to collect sufficient number of samples that are equivalent to those obtained by sampling one frame at a higher rate. We define the equivalent high sampling rate as $1/T_b$, which satisfies the condition $T_b \leq 1/2B$ in order to prevent frequency aliasing. The resolution of TOA estimation is also T_b ($\leq T_{\text{sam}}$). The relationships among T_{sam}, T_f, and T_b are given as follows

$$T_{\text{sam}} = mT_b, \quad (1)$$

$$T_f = (mP + n)T_b, \quad (2)$$

where $m \geq 1$ is the sampling gain, $P = \lfloor T_f/T_{\text{sam}} \rfloor$ is the minimum number of samples collected from one frame and $m > n \geq 0$. These parameters are all integers. Moreover, m and $mP+n$ should be relatively prime. Under the condition of $m = 1$ and $n = 0$, the system becomes the Nyquist sampling system. When designing the sampling gain m, we would like it to be as large as possible to lower the sampling rate. On the other hand, it has to be small to shorten the preamble. There is a design trade-off. Using m frames to collect $mP + n$ samples is equivalent to sampling one frame at rate $1/T_b$. Figure 2(a) shows an example. The waveform $x(t)$ represents the output of the front-end filter. In the example, $m = 3$, $P = 3$ and $n = 2$, which leads to $T_f = (mP + n)T_b = 11T_b$. We collect 11 samples in a time duration of $3T_f$. These samples are equivalent to those obtained by sampling one frame at the output of the front-end filter at rate $1/T_b$, and permuting as shown at the right side of Fig. 2(a).

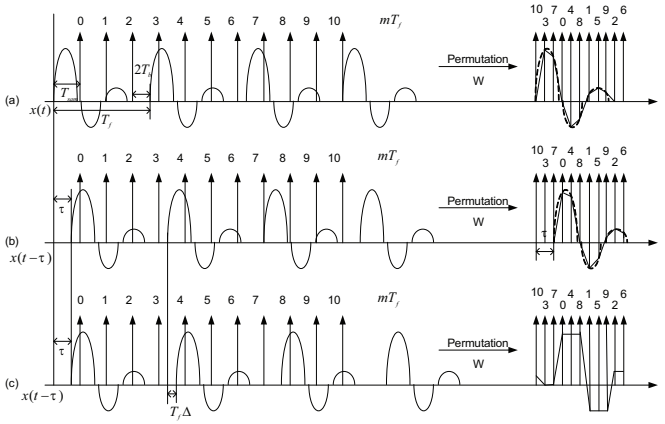

Fig. 2. The noiseless output of the front-end filter at the receiver. (a) The ideal case, no drift and $\tau = 0$, (b) no drift and $\tau \neq 0$ and (c) with drift and $\tau \neq 0$.

The relative clock drift between the transmitter and the receiver voilates the relation in (2). That is because T_f is with respect to the transmitter, while T_{sam} is with respect to the receiver. When we apply stroboscopic sampling at the receiver, we require a long preamble in order to obtain sufficient number of samples. But since the relative clock drift ratio can be as large as 80 ppm [1], the drift of the preamble can lead to serious problems in TOA estimation. For example, a 1 ms preamble would account for an 80 ns clock drift. Therefore, we have to calibrate for the clock drift at the receiver for accurate ranging. Figs. 2(b) and 2(c) indicate examples without and with clock drift, respectively, where Δ is the relative clock drift ratio and τ is the TOA. In Fig. 2(b), the timing information can be retrieved after permuting the sample sequence, whereas in Fig. 2(c) the original waveform can not be recovered due to the clock drift, and the timing information is lost.

We assume the clock drift ratio remains constant. In order to suppress the noise and simplify the problem, we define a group of frames as a cluster, whose duration is smaller than the minimum time period required to observe a drift of T_b. Therefore, relation (2) is roughly maintained within the cluster. Recalling that $1/T_b$ is larger than $2B$, a maximum drift T_b of a cluster is smaller than the width of the pulse. Hence, frame samples can be averaged over the cluster without severe pulse mismatch. We recall that T_b is the resolution for

TOA estimation. The cluster period is defined as $N_f T_f$, where $N_f = mM$. It has to satisfy the following condition [10], [11]

$$N_f T_f \Delta_{\max} = mMT_f \Delta_{\max} \leq T_b, \tag{3}$$

where $M > 0$ is the processing gain, and $\Delta_{\max}$ is the maximum clock drift ratio at the transmitter relative to the receiver. For instance, if the targeted T_b is 1 ns, $T_f = 100$ ns, and $\Delta_{\max}$ is 80 ppm, then $N_f \leq 125$, which means $mM \leq 125$. A proper choice of m could be 9, which indicates a sampling rate of $1/T_{\text{sam}} = 111.1$ MHz or a sampling period of $T_{\text{sam}} = 9$ ns. As a result, the largest processing gain M can be 14. The outcome of the cluster averaging are $mP + n$ samples of one frame.

In order to achieve TOA estimation, we could design the preamble to be composed of several segments, each of which is dedicated to different purposes, such as signal detection, coarse synchronization and fine synchronization. Each segment could have a different structure to facilitate its task. The structural design of the whole preamble is out of the scope of this paper. We assume coarse synchronization has already been carried out. More specifically, we assume that the TOA τ is in the range of one frame period with respect to the receiver, i.e., $\tau \in [0, (1+\Delta)T_f)$, where $(1+\Delta)T_f \approx T_f$, since T_f is only several hundreds of ns and $\Delta \leq 80$ ppm. Therefore, we only concentrate on designing the preamble for the fine synchronization to estimate the τ. We assign a code chip to each cluster instead of each frame in order to avoid code mismatch during the averaging due to the unknown τ and the clock drift, which is not considered in [10], [11]. Based on the analysis above, the structure of the transmitted preamble is shown in Fig. 3(a). The preamble is composed of N_c clusters, where every cluster is made up of N_f frames, each one containing one pulse. The transmitted signal is

$$s(t) = \sum_{i=0}^{N_c-1} c_i \sum_{j=0}^{N_f-1} p(t - (iN_f + j)T_f), \tag{4}$$

where c_i is the cluster code chip and $p(t)$ is the transmitted pulse shape. Figs. 3(b) and 3(c) show the noiseless received preamble through an additive white Gaussian noise (AWGN) channel with unknown τ and different clock drifts. As we can observe from the figures, there is a code mismatch due to the unknown τ and the clock drift. The last several frames of the clusters in Fig. 3(b) are mismatched due to the unknown τ and the negative drift, while the first several frames of the clusters in Fig. 3(c) are mismatched as a result of the unknown τ and the positive drift. We cut off the first and last m frames of the cluster to get rid of the code mismatch in the averaging process at the price of reducing the processing gain from M to $M-2$. As illustrated in the previous example, an 80 ppm drift ratio may cause an 80 ns clock drift for a 1 ms preamble. Due to this drift and the unknown $\tau \in [0, 100\text{ ns})$, the timing offset at the last frame of the preamble will be in the range of $[\tau - 80\text{ ns}, \tau + 80\text{ ns})$, which leads to a timing offset range of $[-80\text{ ns}, 180\text{ ns}]$. The m frames we omit provide a guard time, which is larger than the timing offset range. Hence, it can prevent code mismatch. When $m = 1$, however, the timing offset range is larger than the guard time, and the last frame still suffers from a code mismatch even after frame removal. Nevertheless, since we average lots of frames over the cluster in case $m = 1$, a code mismatch in one frame does not introduce a big influence. The received preamble is

$$r(t) = \sum_{i=0}^{N_c-1} c_i \sum_{j=0}^{N_f-1} h(t-(iN_f+j)T_f(1+\Delta)-\tau)+n(t), \tag{5}$$

where Δ is the clock drift ratio, $h(t) = h_p(t) \star p(t)$ of length $T_h < T_f$ is the aggregate channel, with $p(t)$ the transmitted pulse and $h_p(t)$ the UWB physical multipath channel, and $n(t)$ is the zero-mean AWGN with double sided power spectral density $N_0/2$. We assume $h_p(t) = \sum_{l=0}^{L-1} \alpha_l \delta(t - \tau_{l,0})$, where L indicates the number of multipath components, and α_l and $\tau_{l,0}$ represent the amplitude and the relative time delay of the lth path with respect to the first path, respectively. It is obtained by $\tau_{l,0} = \tau_l - \tau_0$, where τ_i is the multipath delay and $\tau_0 = \tau$ is the TOA. With the received signal $r(t)$, the output of the front-end filter is

$$x[k] = \int_{-\infty}^{+\infty} r(t) g(kT_{\text{sam}} - t) dt, \quad k = 0, 1, \ldots, \tag{6}$$

where $g(t)$ is the impulse response of the front-end filter, whose bandwidth is large enough to include the band of interest. We define $L_f = T_f/T_b = mP + n$ as the frame length in terms of the number of samples at rate $1/T_b$ and $\mathbf{x}_k = [x[kL_f], x[kL_f + 1], \ldots, x[(k+1)L_f - 1]]^T$, which is an L_f-long sample vector for the kth equivalent frame. Notice that $\mathbf{x}_k$ is the result of sampling m frames at rate $1/T_{\text{sam}}$ at the receiver. Further, the samples are divided into clusters. We exclude the first and last sample vectors in each cluster to get rid of the code mismatch in the averaging process. The results are collected in a data matrix $\mathbf{X}$ of size $L_f \times N_c$ as

$$\mathbf{X} = \frac{1}{M-2} \left[\sum_{k=1}^{M-2} \mathbf{x}_k \;\; \sum_{k=1}^{M-2} \mathbf{x}_{M+k} \;\; \cdots \;\; \sum_{k=1}^{M-2} \mathbf{x}_{(N_c-1)M+k} \right], \tag{7}$$

where each column of $\mathbf{X}$ contains its own specific code chip.

III. TOA ESTIMATION WITH CLOCK DRIFT CALIBRATION

A. Recovery from stroboscopic sampling

Due to the stroboscopic effects, we have to permute all the averaged frame samples in each column of $\mathbf{X}$ before we calibrate for the drift and estimate the TOA τ. The adjacent T_{sam}-spaced samples obtained by stroboscopic sampling are not the adjacent T_b-spaced samples in the equivalent high sampling rate scheme as shown in Fig. 2(a). The maximum drift observed in a cluster is T_b, which is much smaller than the sample spacing T_{sam} in the stroboscopic sampling scheme, and exactly equal to the sample spacing in the equivalent high sampling rate scheme. Therefore, we have to recover the equivalent high sampling rate sequence before drift calibration in order to observe the drift between the adjacent clusters.

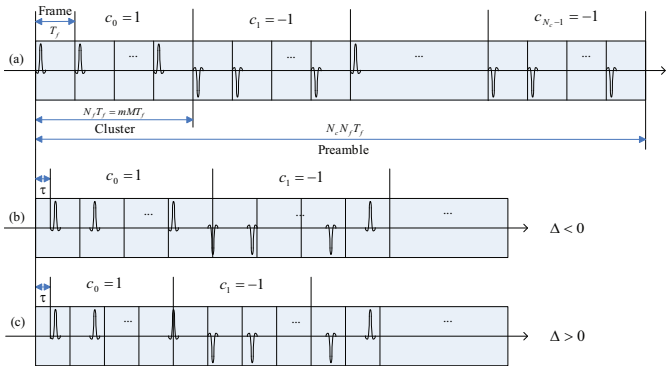

Fig. 3. The structure of (a) the preamble, (b) the received preamble with negative drift and (c) the received preamble with positive drift.

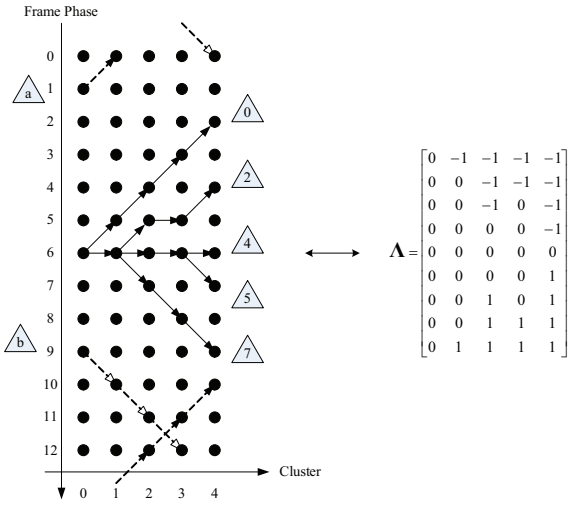

Fig. 4. The diagram of the transition paths and the matrix $\mathbf{\Lambda}$, $N_c = 5$ and $L_f = 13$.

According to (2), we define a permutation matrix $\mathbf{W}$ of size $L_f \times L_f$, whose first row is $\mathbf{W}(1,:) = [\mathbf{0}_{m-1}^T, 1, \mathbf{0}_{L_f-m}^T]$. Further, every row is a circulant shift of the previous row, which means that

$$\mathbf{W}(i+1,:) = \{\text{circshift}(\mathbf{W}(i,:)^T, m)\}^T, i = 1, \ldots, L_f - 1, \tag{8}$$

where circshift$(\mathbf{a}, n)$ circularly shifts the values in the vector $\mathbf{a}$ by $|n|$ elements (down if $n > 0$ and up if $n < 0$). Since $\mathbf{W}$ is a permutation matrix, we have $\mathbf{W}\mathbf{W}^T = \mathbf{I}$ and $\mathbf{W}^{-1} = \mathbf{W}^T$. The rearrangement is accomplished by

$$\mathbf{X}_o = \mathbf{W}^T\mathbf{X}, \tag{9}$$

where each column of $\mathbf{X}_o$ collects the permuted averages for each cluster. Now, the equivalent sample spacing in $\mathbf{X}_o$ is T_b.

B. Maximum likelihood estimator of clock drift

In order to estimate the TOA, we would like to use all the data samples in $\mathbf{X}_o$. This allows us to obtain an averaged sample vector over all the clusters and thereby reduces the noise. However, due to the clock drift, the equivalent frame waveforms do not align with each other. We have to calibrate for the drift before TOA estimation. Let us define the row index of the data matrix $\mathbf{X}_o$ as the frame phase, similar to the pulse repetition period (PRP) phase in [10], [11]. We recall that the maximum drift observed over a cluster duration is T_b, which means that the frame phase of a cluster may correspond to the same or an adjacent phase in the next cluster. This kind of correspondence is called the transition between frame phases. The drift estimation traces the correct transition path of the frame phase within the duration of the preamble. A transition takes place between two contiguous clusters, and the step for each transition could be zero or one frame phase. Every frame phase has the same set of transition paths. We remark that the exact number of the drift ratio is not the main concern, but the transition path is the target of the drift estimation. Based on this path, we can calibrate for the drift, obtain an averaged sample vector for the whole preamble, and then estimate the TOA. The resolution of the drift estimation is $\Delta_{\max}/(N_c - 1)$. The total number of transition paths for each frame phase is $2N_c - 1$. Therefore, the longer the preamble, the more accurate the drift estimation. Nevertheless, the complexity of the estimation would also increase as the number of transition paths increases.

Fig. 4 shows some examples of transition paths. In the example, $N_c = 5$ and $L_f = 13$. The dots represent the elements of the matrix $\mathbf{X}_o$. The spacing between contiguous samples is T_b. Based on Fig. 4, we reconfirm that the data matrix $\mathbf{X}$ can not be used directly. Some of the transition paths for frame phase 6 are shown. Path 0 indicates that we can observe a phase transition for every cluster, and the kth phase of the ith cluster transfers to the $(k-1)$th phase of the $(i+1)$th cluster. It reaches the negative maximum drift. Path 2 denotes one transition for every two clusters. Both of the paths indicate negative drift. In path 4, no clock drift is observed. Path 5 shows one transition for every four clusters, which corresponds to a resolution of the drift ratio estimation given by $\Delta_{\max}/4$. Finally, path 7 shows three transitions for every four clusters. The last two paths show positive drift. The number of all possible transition paths for each frame phase is $2N_c - 1 = 9$. There are special cases we have to be careful with. For example, in path a for phase 1, there is a negative shift of one phase every cluster. Therefore, phase 0 of cluster 1 transfers to phase 12 of cluster 2 as shown by the dashed line with solid arrow in the figure. Meanwhile, path b for phase 9 describes a positive shift of one phase every cluster. Hence, as denoted by the dashed line with hollow arrow in Fig. 4, phase 12 of cluster 3 transfers to phase 0 of cluster 4. The transition takes place circulantly. We have excluded the code mismatch during the cluster averaging process by cutting off the first and last sample vectors. However, the phase mismatch due to the clock drift still causes serious problems for TOA estimation.

All the transition paths for any phase are modeled in a matrix $\mathbf{\Lambda}$ of size $(2N_c - 1) \times N_c$. For instance, $\mathbf{\Lambda}$ for $N_c = 5$ is shown at the right side of Fig. 4. The path number in Fig. 4 corresponds to the row index of $\mathbf{\Lambda}$. Making use of the transition matrix and recalling the cluster code, we carry

out a maximum-likelihood search for the clock drift and the strongest multipath component jointly [10], [11].

$$[k_{\max}, j_{\max}] = \arg\max_{k,j} \left| \sum_{n=0}^{N_c-1} c_n \mathbf{X}_o(p,n) \right|, \quad (10)$$

$$k \in \{0, \ldots, L_f - 1\},$$

$$j \in \{0, \ldots, 2N_c - 2\},$$

$$p = \mathrm{mod}\big((k + \sum_{i=0}^{n} \mathbf{\Lambda}(j,i)), L_f\big), \quad (11)$$

where $k_{\max}$ represents the index of the strongest multipath component and $j_{\max}$ is the row index of the selected path in $\mathbf{\Lambda}$. The function $\mathrm{mod}(a,b)$ computes a modulo b. Since all the phases have the same set of transition paths, we can also process the maximum-likelihood search for the transition path, which collects the maximum energy over the whole preamble in order to be more robust to noise. This leads to

$$j'_{\max} = \arg \max_{j \in \{0,\ldots,2N_c-2\}} \sum_{k=0}^{L_f-1} \left\| \sum_{n=0}^{N_c-1} c_n \mathbf{X}_o(p,n) \right\|_F^2, \quad (12)$$

where $j'_{\max}$ is also the row index of the selected path in $\mathbf{\Lambda}$ and p is computed in the same way as (11).

C. TOA estimation

Until now, we have estimated the transition path for the clock drift using two methods, (10) and (12). The index of the strongest multipath component is obtained at the same time by (10). Thus, the TOA estimation according to peak selection [5], [6] is given by $\hat{\tau}_p = k_{\max} T_b$, as a result of (10). In a non-line-of-sight (NLOS) scenario, the first path may not be the strongest path. Therefore, we resort to the leading edge detection [5], [6] to find the index of the first frame phase, whose absolute value is larger than a threshold.

Consequently, we average related phases of $\mathbf{X}_o$ over the whole preamble according to the transition path $\mathbf{\Lambda}(j_{\max}, :)$ to calibrate for the drift and further mitigate the noise, and collect the outcomes in a sample vector $\mathbf{y}$, whose elements are computed as:

$$y[k] = \frac{1}{N_c} \sum_{n=0}^{N_c-1} c_n \mathbf{X}_o(p_{\max}, n), k = 0, 1, \ldots, L_f - 1, \quad (13)$$

where $p_{\max}$ is obtained by plugging $\mathbf{\Lambda}(j_{\max}, :)$ into (11). The sample vector $\mathbf{y}'$ is obtained in the same way using $j'_{\max}$. The vector $\mathbf{y}$ ($\mathbf{y}'$) is used for TOA estimation. As a result, the total processing gain for TOA estimation is $N_c(M-2)$. We carry out the leading edge detection by first finding the index of the strongest component, where $k_{\max}$ is already obtained by (10) and $k'_{\max} = \max |y'[k]|, k = 1, \ldots, L_f - 1$. Secondly, a threshold γ (γ') is selected and a backward search window of length L_w is defined. Finally, we execute a backward search starting from $k_{\max}$ (k'_{max}) to find out the index of the first $|y[k]|$ ($|y'[k]|$) exceeding the threshold inside the window. The threshold can be derived by analyzing the stochastic properties of $\mathbf{y}$ ($\mathbf{y}'$) and then applying detection theory. In the absence of channel information, we follow a heuristic approach and set the threshold to $\gamma = \eta_t |y[k_{\max}]|$ ($\gamma' = \eta_t |y'[k'_{\max}]|$), where $0 \leq \eta_t \leq 1$ is the threshold ratio. The length L_w of the backward search window depends on the characteristics of the multipath channel. It should be small enough to avoid the case where we mistakenly regard the channel tail as the first path, whereas it should be large enough to recover the first path instead of the deadlock to the strongest one. However, due to the lack of channel knowledge, we choose L_w to be $\eta_l T_f$, where $0 \leq \eta_l \leq 1$ is the length ratio.

IV. Simulation results

The performance of TOA estimation is evaluated by simulations using the IEEE 802.15.4a channel model CM1 - indoor residential LOS [12]. The channel impulse responses are truncated to 90 ns to avoid IFI. One-hundred channel realizations are generated, and we randomly choose one in each Monte Carlo run. To speed up the simulation, we generate the output of the cluster averaging process directly. E_c/N_o defines the cluster energy to noise variance ratio. The number of clusters N_c is 65. Further, we randomly select the drift ratio Δ among $\{-64.8$ ppm, -43.2 ppm, -21.6 ppm, 0 ppm, 21.6 ppm, 43.2 ppm, 64.8 ppm$\}$ in each run. The frame period T_f is 100 ns. The stroboscopic sampling period T_{sam} is 9 ns. The targeted resolution T_b is 1 ns. Based on (2), we obtain $P = 11$, $m = 9$ and $n = 1$. The maximum M is 17 according to (3). Therefore, the processing gain of the cluster averaging process is $M - 2 = 15$, or approximately 11 dB. The total processing gain is $N_c(M-2) = 975$, or approximately 30 dB. The second derivative of a Gaussian pulse is employed as the transmitted pulse, and the pulse width is truncated to 4 ns, which includes the main lobe and two side lobes. Its bandwidth is approximately 500 MHz. The pulse is also used as the impulse response of the front-end filter at the receiver. Moreover, the timing offset $\tau \in [0, T_f)$ is randomly generated in each run. The threshold ratio is $\eta_t \in \{0.1, 0.2 \ldots, 0.9\}$. The length ratio of the backward search window is $\eta_l \in \{0.1, 0.3, 0.5\}$, which leads to $L_w \in \{10$ ns, 30 ns, 50 ns$\}$.

We first evaluate the performance of TOA estimation using the peak selection method. The root mean square error (RMSE) of $\hat{\tau}_p$ vs. E_c/N_o is illustrated in Fig. 5. There are large performance gaps between the cases with drift calibration (solid lines) and the cases without drift calibration (dashed lines). The drift causes serious problems to TOA estimation as indicated by the high error floor for the curves without calibration. (10) and (12) have almost the same performance. The Nyquist sampling system, where $m = 1$ and $n = 0$, is used as a reference. No matter how large m, the RMSE of TOA estimation with drift calibration always converges to the same error floor. Nyquist sampling gains about 10 dB over stroboscopic sampling ($m = 9$) due to the sampling gain m. For both systems, we also show the performance of the ideal case without any drift. They show similar error floors as the ones with drift calibration, which proves that the drift is not the reason for the error floor. It is probably due to the fact we

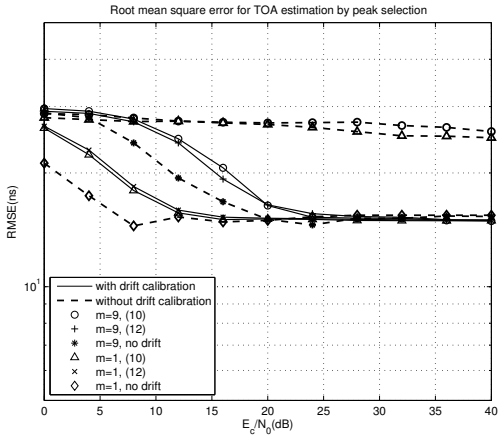

Fig. 5. RMSE of TOA estimation by peak selection.

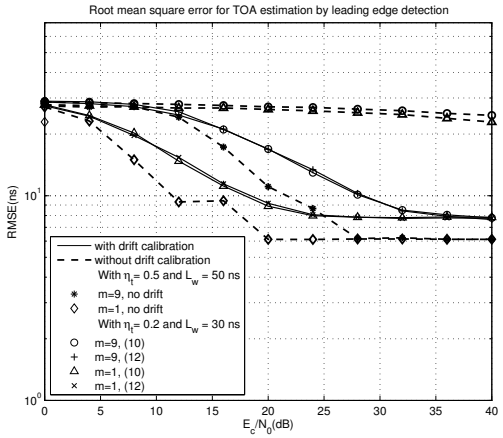

Fig. 6. RMSE of TOA estimation by leading edge detection.

employ a signal with a bandwidth of 500 MHz, which may not be enough to resolve fine multipaths. Since there is inter-pulse interference (IPI), the peak selection method always chooses the strongest resolvable signal component instead of the strongest single path, which causes a high error floor. We may improve the performance of the peak selection method by employing a signal with a larger bandwidth.

We also investigate the performance of TOA estimation by leading edge detection as shown in Fig. 6, which achieves much better accuracies than the peak selection method. Fig. 6 illustrates the best performance of TOA estimation for different combinations of thresholds and search windows. The results without drift calibration (dashed lines) are much worse than the ones with drift calibration (solid lines). The drift calibration dramatically reduces the TOA estimation error due to the drift. Nyquist sampling is still used as a reference and performs the best. There are small error floor differences between the cases with drift calibration and the ideal cases without any drift. The best combination of the threshold and the search window among all the tested combinations is $\eta_t = 0.2$ and $L_w = 30$ ns. However, the error floors still remain. In order to improve the performance of the leading edge detection, we need to analysis the stochastic properties of $\mathbf{y}$ ($\mathbf{y}'$) to set an optimal threshold, and obtain some prior knowledge about the multipath channel to make a proper backward search window.

V. Conclusions

In this paper, we have applied stroboscopic sampling for an IR-UWB system to achieve accurate TOA estimation with a low sampling rate. Due to the long preamble required by stroboscopic sampling, the clock drift is one of the main error sources in TOA estimation. Hence, we include the drift into our system model and obtain a maximum-likelihood estimation. Further, we carry out the peak selection and the leading edge detection to estimation the TOA using the averaged data samples corrected for the drift. Simulation results confirm that the drift calibration dramatically reduces the TOA estimation errors due to the drift, and stroboscopic sampling can achieve the same estimation resolution as Nyquist sampling. We have proposed a practical low sampling rate solution for TOA estimation using UWB signals.

References

[1] IEEE Working Group 802.15.4, "Part 15.4: Wireless Medium Access Control (MAC) and Physical Layer (PHY) Specifications for Low-Rate Wireless Personal Area Networks (LR-WPANs)," Dec. 2006.

[2] S. Gezici, Z. Tian, G. Giannakis, H. Kobayashi, A. Molisch, H. Poor, and Z. Sahinoglu, "Localization via ultra-wideband radios: a look at positioning aspects for future sensor networks," *IEEE Signal Process. Mag.*, vol. 22, pp. 70–84, July 2005.

[3] J.-Y. Lee and R. Scholtz, "Ranging in a dense multipath environment using an UWB radio link," *IEEE J. Sel. Areas Commun.*, vol. 20, no. 9, pp. 1677–1683, Dec. 2002.

[4] Z. Sahinoglu and S. Gezici, "Ranging in the IEEE 802.15.4a standard," in *IEEE Annu. Wireless and Microwave Technology Conf. (WAMICON '06)*, Clearwater Beach, Fla, USA, Dec. 2006, pp. 1–5.

[5] I. Guvenc, Z. Sahinoglu, and P. Orlik, "TOA estimation for IR-UWB systems with different transceiver types," *IEEE Trans. Microw. Theory Tech.*, vol. 54, no. 4, pp. 1876–1886, Jun. 2006.

[6] C. Falsi, D. Dardari, L. Mucchi, and M. Win, "Time of arrival estimation for UWB localizers in realistic environments," *EURASIP Journal on Applied Signal Processing*, pp. 1–13, 2006.

[7] W. Chung and D. Ha, "An accurate ultra wideband (UWB) ranging for precision asset location," in *Proc. IEEE Conf. UWB Systems & Technologies*, Reston,VA, Nov. 2003, pp. 389–393.

[8] R. Zhang and X. Dong, "A new time of arrival estimation method using UWB dual pulse signals," *IEEE Trans. Wireless Commun.*, vol. 7, no. 6, pp. 2057–2062, Jun. 2008.

[9] Z. Irahhauten, A. Yarovoy, G. Janssen, H. Nikookar, and L. Ligthart, "Suppression of noise and narrowband interference in UWB indoor channel measurements," in *Proc. IEEE Int. Conf. Ultra-Wideband*, Sept. 2005, pp. 108–112.

[10] A. Wellig and Y. Qiu, "Trellis-based maximum-likelihood crystal drift estimator for ranging applications in UWB-LDR," in *Proc. IEEE Int. Conf. Ultra-wideband*, Sept. 2006, pp. 539–544.

[11] A. Wellig, "Method and device for estimation the relative drift between two clocks, in particular for ranging applications in UWB-LDR technology," U.S. Patent 2008/0 069 260A1, Mar. 20, 2008.

[12] A. Molisch, K. Balakrishnan, C. Chong, S. Emami, A. Fort, J. Karedal, J. Kunisch, H. Schantz, U. Schuster, and K. Siwiak, "IEEE 802.15.4a channel model-final report," Tech. Rep., 2005.